Acta Crystallographica Section D
Biological Crystallography
ISSN 0907-4449

X-ray structure of p38α bound to TAK-715: comparison with three classic inhibitors

Rita Azevedo,[a,b] Mario van Zeeland,[a,c] Hans Raaijmakers,[a,c] Bert Kazemier,[a] Jacob de Vlieg[a,b] and Arthur Oubrie[a,c]*

[a]Merck Research Laboratories, MSD, PO Box 20, 5340 BH Oss, The Netherlands, [b]CMBI, Radboud University Nijmegen Medical Centre, Geert Grooteplein Zuid 26-28, 6525 GA Nijmegen, The Netherlands, and [c]Lead Pharma Medicine, Kapittelweg 29, 6525 EN Nijmegen, The Netherlands

Correspondence e-mail: arthur.oubrie@leadpharma.com

Received 11 January 2012
Accepted 3 May 2012

PDB References:
p38α–SB-203580, 3zs5; p38α–TAK-715, 3zsg; p38α–SCIO-469, 3zsh; p38α–VX-745, 3zsi.

The p38α mitogen-activated protein kinase regulates the synthesis of pro-inflammatory cytokines in response to stimulation by a diverse set of stress signals. Various different chemotypes and clinical candidates that inhibit p38α function have been reported over the years. In this publication, the novel structure of p38α cocrystallized with the clinical candidate TAK-715 is reported. Owing to the impact of crystallization conditions on the conformation of protein kinases (and in particular p38α), the structures of complexes of p38α with SB-203580, SCIO-469 and VX-745 have also been determined to enable in-depth comparison of ligand-induced protein conformations. The impact of experimental conditions on p38α–inhibitor complex structures, most importantly soaking *versus* cocrystallization, is discussed. Analysis of the structures and quantification of the protein–ligand interactions couples ligand-induced protein conformations to the number of interactions and to inhibitor selectivity against the human kinome. This shows that for the design of novel kinase inhibitors, selectivity is best obtained through maximization of the number of interactions throughout the ATP pocket and the exploitation of specific features in the active site.

1. Introduction

The p38α mitogen-activated protein kinase (MAPK) pathway regulates various cellular processes, including inflammation, immune response, cell survival and differentiation (Han *et al.*, 1994; Lee *et al.*, 1994). The pathway is activated upon stimulation by a diverse set of extracellular stress signals including bacterial endotoxic lipopolysaccharide (LPS), heat shock, osmotic stress, arsenite and cytokines (Han *et al.*, 1994, 1997; Rouse *et al.*, 1994; Freshney *et al.*, 1994). The pathway controls the production and secretion of pro-inflammatory cytokines such as tumour necrosis factor-α (TNFα), interleukin-6 (IL-6) and interleukin-1β (IL-1β), amongst others (Lee *et al.*, 1994). Selective inhibition of any of these three cytokines using antibody therapies has shown efficacy both in animal models and in the clinical setting for the treatment of autoimmune diseases such as rheumatoid arthritis (RA) and psoriasis (Maini *et al.*, 1999; Nishimoto *et al.*, 2009).

Owing to its central role in the regulation of cytokine production and inflammatory disease, many pharmaceutical companies have actively pursued p38α as a drug target. Some disappointing clinical data have led many to conclude that

p38α inhibitors are not suitable for the treatment of RA (Genovese, 2009; Hammaker & Firestein, 2010). However, one highly selective p38α inhibitor, PH-797804, was recently reported to have demonstrated efficacy over the entire six-week time course of a Phase II clinical trial for the treatment of chronic obstructive pulmonary disease (COPD; MacNee *et al.*, 2010). The discovery that inhibition of p38α activity has potential for the anti-inflammatory treatment of COPD is likely to trigger renewed interest in modulating the activity of the p38α signalling pathway using small-molecule inhibitors. In order to contribute to the development of novel leads and candidates, we sought to compare the binding characteristics of various p38α clinical candidates and other classical inhibitors, including TAK-715.

TAK-715 has been reported to demonstrate strong inhibitory activity in cell-based assays, good bioavailability in mice and rats, and significant efficacy in a long-term disease model, *i.e.* rat adjuvant-induced arthritis. A specific feature of this compound is its lack of inhibition of cytochrome P450s, with the potential to lower the risk of drug–drug interactions and hepatotoxicity (Miwatashi *et al.*, 2005). The compound has been tested in a Phase II clinical trial for the treatment of RA (http://clinicaltrials.gov/ct2/show/NCT00760864). The study has been completed, but the results have not yet been communicated.

Various X-ray structures have been published of p38α in different functional and pharmacologically relevant states, *i.e.* from nonphosphorylated ligand-free forms *via* (phosphorylated) substrate peptide-bound states to nonphosphorylated conformations bound to many different small-molecule inhibitors (Wilson *et al.*, 1996; Wang *et al.*, 1997; Chang *et al.*, 2002; Akella *et al.*, 2010). NMR structural data have also been obtained, but only 64% of the backbone could be assigned, which was attributed to flexibility of the catalytic C-helix, activation loop and C-terminal subdomains (Vogtherr *et al.*, 2005, 2006). The combined structural data illustrate that p38α exhibits considerable protein flexibility, even for a protein kinase, as the hinge, Gly-rich loop, activation loop, catalytic helix, peptide-docking groove and p38α-specific insert can all adopt several different conformational states.

Previous structures of p38α bound to SB-203580 (Tong *et al.*, 1997; Wang *et al.*, 1998; Vogtherr *et al.*, 2006; Simard *et al.*, 2009) show that the binding conformation (Fig. 1) can differ substantially depending on the experimental conditions. For example, PDB entry 1a9u (Wang *et al.*, 1997) shows the DFG segment in its active DFG-in conformation and PDB entry 3gcp (Simard *et al.*, 2009) shows the inactive DFG-out fold, whilst PDB entry 2ewa (Vogtherr *et al.*, 2006) presents both conformations. PDB entries 1a9u and 2ewa result from soaking experiments with relatively different conditions, whilst PDB entry 3gcp was produced by cocrystallization of the protein with the ligand. It is clear that for a fair comparison of different p38α–inhibitor complexes similar conditions should be used to produce the various structures. We therefore report the novel structure of p38α cocrystallized with TAK-715, as well as new high-resolution structures of p38α bound to SB-203580, SCIO-469 and VX-745. As the experimental conditions are similar for all cocrystals, an unbiased comparison of the binding features of each of the ligands is possible. The impact of these conditions is evaluated.

The X-ray structures point to marked conformational flexibility of the p38α protein. This structural information was combined with publicly available protein kinase selectivity profiles and contact-residue information to generate an in-depth understanding of the relationships between compound chemical structure, compound-induced protein conformation and selectivity.

2. Experimental procedures

2.1. Cloning, expression and purification

The crystallization construct was amplified from human p38α cDNA with N- and C-termini as described previously (Wang *et al.*, 1997). p38α was cloned in a Gateway-adapted expression vector (derived from pMal-c2x, NEB) with an N-terminal His tag followed by a thrombin protease cleavage site. The purified protein sequence starts with a Gly-Ser-His thrombin cleavage-tag remnant followed by the p38 sequence (UniProt Q16539, MK14_HUMAN) starting at Ser2 and containing all residues up to the natural C-terminus. After thrombin cleavage, the N-terminal sequence starts with GSHSQERPT. The expression vector was transformed into *Escherichia coli* BL21 (DE3) cells to express the recombinant fusion protein. During subsequent optimization tests, the construct was transformed into the *E. coli* Rosetta (DE3) strain, which gave improved protein yields. To express the recombinant protein, a starter culture was grown overnight in 50 ml minimal medium containing 20 μg ml^{-1} chloramphenicol and 100 μg ml^{-1} ampicillin. The next day, this preculture was used to inoculate a 4 l fermentor filled with standard medium and 100 mg l^{-1} ampicillin. The culture was grown at 303 K to an OD_{640} of 24, after which the temperature

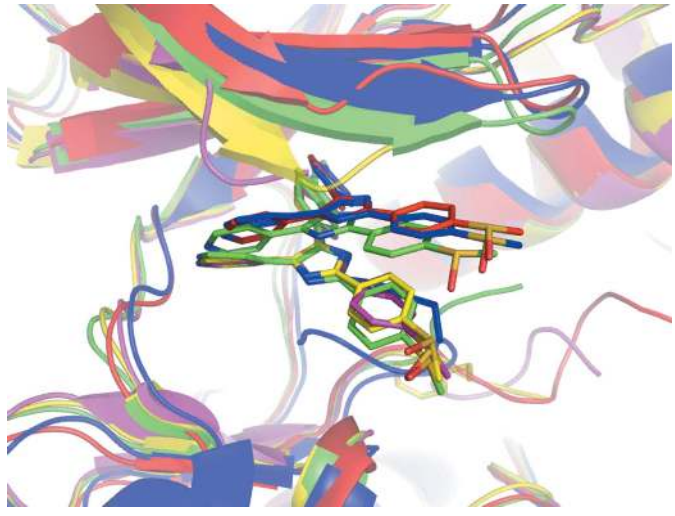

Figure 1
Comparison of the binding conformation of SB-203580 in previously published structures: PDB entry 1a9u, red; PDB entry 2ewa, green; PDB entry 3gcp, blue; PDB entry 3mpa, yellow; PDB entry 3obg, magenta.

Table 1
Data-collection and refinement statistics.

Values in parentheses are for the highest resolution shell.

Data set	SB-203580	TAK-715	SCIO-469	VX-745
Data collection				
Space group	$P2_12_12_1$	$P2_12_12_1$	$P2_12_12_1$	$P2_12_12_1$
Unit-cell parameters (Å)	a = 67.49, b = 70.04, c = 75.01	a = 68.54, b = 70.17, c = 74.76	a = 68.72, b = 70.08, c = 74.29	a = 65.55, b = 73.65, c = 76.57
Resolution (Å)	1.60 (1.69–1.60)	1.89 (2.00–1.89)	1.93 (2.04–1.93)	2.01 (2.12–2.01)
$R_{\rm merge}$†	0.082 (0.88)	0.065 (0.45)	0.096 (0.94)	0.105 (1.561)
Mean $I/\sigma(I)$	8.0 (0.8)	9.6 (1.6)	7.1 (0.8)	6.6 (0.5)
Completeness (%)	93.8 (75.3)	100.0 (100.0)	99.2 (96.6)	96.8 (89.9)
Multiplicity	6.9 (5.9)	6.2 (6.1)	4.6 (4.5)	4.4 (4.2)
Refinement				
Resolution (Å)	51–1.60	35–1.89	37–2.05	38–2.40
No. of reflections	42175	27922	21887	14272
$R_{\rm work}/R_{\rm free}$ (%)	18.34/21.58	18.93/23.30	20.54/25.51	23.06/27.07
No. of non-H atoms				
Total	3191	3138	2973	2882
Protein	2825	2772	2711	2704
Inhibitor	27	29	36	28
Octyl glucoside	36	20	20	20
Solvent	303	317	206	130
Average B factor (Å^2)				
Overall	22.5	23.8	31.7	16.5
Protein	21.8	22.7	31.0	16.0
Inhibitor	22.9	27.3	42.8	41.1
Octyl glucoside	31.2	30.5	41.5	44.0
Solvent	28.0	32.4	36.7	18.2
R.m.s.d.				
Bond lengths (Å)	0.011	0.009	0.012	0.005
Bond angles (°)	1.4	1.2	1.3	0.88

† $R_{\rm merge} = \sum_{hkl}\sum_i |I_i(hkl) - \langle I(hkl)\rangle| / \sum_{hkl}\sum_i I_i(hkl)$ (Evans, 2006).

was lowered to 293 K and additional sorbitol and 0.3 m*M* IPTG were added. After 4 h, at an OD_{640} of 33, the cells were harvested by centrifugation at 6000 rev min^{-1} for 30 min in a Sorvall GS3 rotor and the cell pellets were stored at 253 K.

The bacterial pellet was suspended in lysis buffer and disrupted in a high-pressure liquid homogenizer (Avestin; two runs at 120 kPa). The lysate was cleared by a 40 min spin at 20 000 rev min^{-1} in a Sorvall centrifuge with an SS34 rotor. The supernatant was applied onto Ni–NTA agarose beads (Qiagen) and His-p38α was eluted with 250 m*M* imidazole in lysis buffer. The His tag was removed by thrombin cleavage and the protein was further purified by anion-exchange chromatography (Mono Q HR 10/100 GL, GE Healthcare). The final polishing step was performed by size-exclusion chromatography on a Superdex 75 column (XK 16/60, GE Healthcare). High-purity peak fractions were pooled and concentrated to 18 mg ml^{-1} (as determined from the A_{280}). Protein in 20 m*M* HEPES pH 7.1, 50 m*M* NaCl, 10 m*M* DTT, 5% glycerol, 0.1 g l^{-1} methionine was flash-cooled in dry ice/ethanol and stored at 203 K.

2.2. Crystallization and data collection

The previously described crystallization conditions (Bukhtiyarova *et al.*, 2004) were optimized for cocrystallization with inhibitors using our batch of protein. Inhibitor stocks were freshly made by dissolving dry powder in 100% DMSO to 100 m*M* final concentration. The inhibitor stock was added to the protein in a threefold molar excess and incubated on ice for at least 10 min. p38α was cocrystallized using the hanging-drop vapour-diffusion method in pre-greased VDX plates (Hampton Research) on siliconized cover slides at room temperature. The crystals grew in 0.1 *M* MES pH 6.5, 19–28% PEG 4000, 50–100 m*M* *N*-octyl-β-D-glucoside, 0–5 m*M* DTT to typical dimensions of 300 × 70 × 60 µm. The crystals were cryoprotected using 20–25% ethylene glycol in the crystallization condition. Crystals cocrystallized with SB-203580 were flash-cooled in liquid nitrogen and a high-resolution data set was collected at the ESRF on a fixed-wavelength beamline (0.933 Å) using an ADSC Q4 CCD detector. Crystals cocrystallized with TAK-715, SCIO-469 and VX-745 were cooled in the cryostream of an in-house X-ray

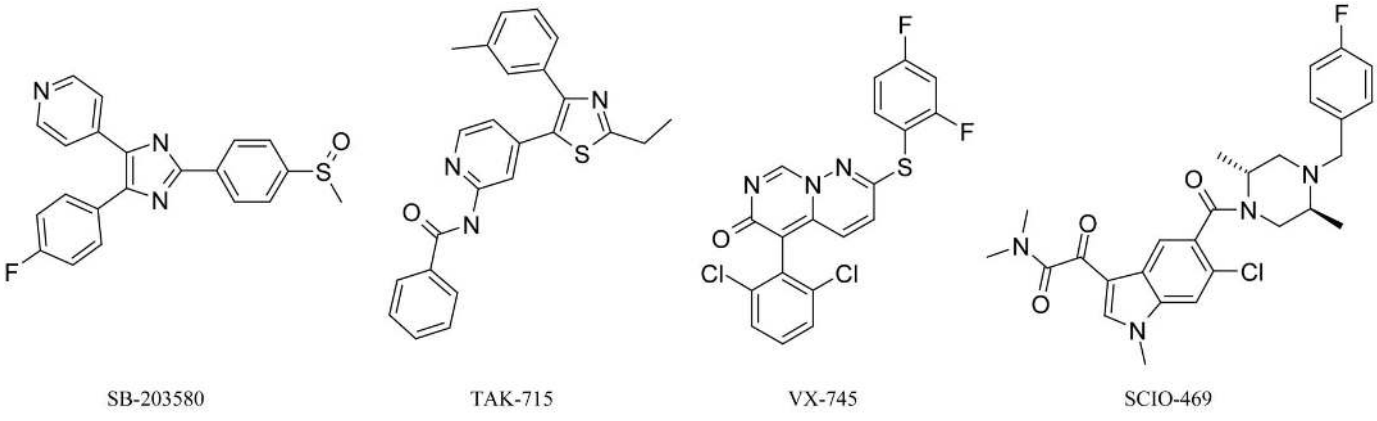

Figure 2
Chemical structures of the four cocrystallized p38α inhibitors.

generator (Rigaku MicroMax-007 HF) and the data were collected using an R-AXIS IV^{++} image-plate detector. Data-collection statistics are given in Table 1.

2.3. Structure determination

X-ray diffraction data were processed with *MOSFLM* and *SCALA* from the *CCP*4 package (Winn *et al.*, 2011). All four structures were determined by rigid-body refinement, using a structure of p38α from an undisclosed but well refined 1.5 Å resolution p38α structure stripped of solvent and inhibitor as a starting model. No further repositioning with molecular-replacement programs was needed. The structural models were adjusted by several rounds of manual model building using *Coot* (Emsley & Cowtan, 2004) and positional refinement using *REFMAC* (Murshudov *et al.*, 2011). Water molecules were added using the *Coot* Find Waters routine within *CCP*4 and were inspected manually using *Coot*. A total of 5% of the observations were excluded from refinement and used for calculation of the $R_{\rm free}$ factor (Brünger, 1992). Refinement statistics and the quality of the structures are summarized in Table 1.

2.4. Structure comparisons, contact-residue identification and frequency determination

Structure comparisons were made using Merck's in-house Protein Kinase Structure Database (publication in preparation) containing all public domain protein kinase structures. Analyses of structures in this database was used to perform comparisons between features seen in the structures presented here and those in other public domain structures.

All structures were imported into *YASARA* (Krieger *et al.*, 2002), where any heteroatoms other than the four inhibitors were deleted. For each of the complexes, a radius of 4 Å was used to identify any residue in possible contact with the ligand. The position of each of these residues was mapped onto the human eukaryotic protein kinase (ePK) multiple sequence alignment (MSA; Manning *et al.*, 2002), which was obtained *via* http://kinase.com. The relative frequency of the p38α

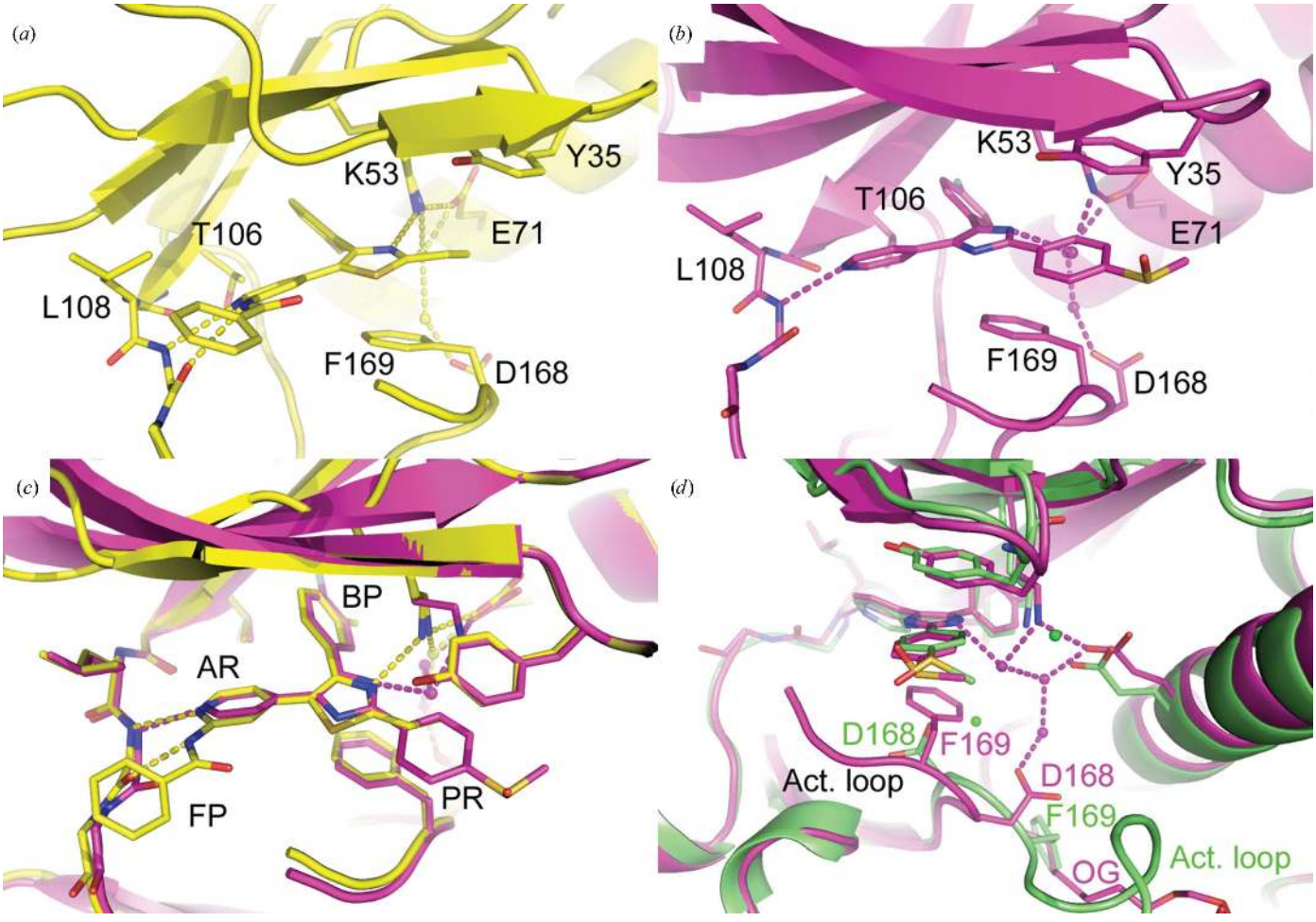

Figure 3
Structures of p38α bound to SB-203580 and TAK-715. Inhibitors and specific amino acids are shown in stick representation and labelled throughout the figure. Hydrogen-bonding interactions are indicated by dotted lines. (*a*) ATP pocket of p38α with bound TAK-715. (*b*) ATP pocket of p38α with bound SB-203580. (*c*) Superposition of structures with SB-203580 and TAK-715. The adenine and phosphate-binding regions (AR and PR) and the front and back pockets (FP and BP) are labelled. (*d*) Superposition of structures with SB-2032580 presented here and from the public domain (PDB entry 1a9u; green). Specific residues are labelled to indicate conformational differences. The activation loops in both structures are labelled.

amino acids at each specific position in the ePK MSA was calculated. All selected residues and their corresponding frequencies of occurrence in the kinome are summarized in Fig. 6.

3. Results and discussion

3.1. Overall structures of p38α–inhibitor complexes

Structures have been determined of p38α bound to TAK-715 and the three classic inhibitors SB-203580, VX-745 and SCIO-469. The chemical structures of these compounds are shown in Fig. 2. Overall, the four protein structures are similar. The SCIO-469 and TAK-715 complexes have r.m.s.d.s from the p38α–SB-203580 complex of 0.369 and 0.138 Å, respectively. The p38α–VX-745 complex shows larger changes in orientation between lobes compared with the SB-203580-bound structure, with overall, N-terminal lobe and C-terminal lobe r.m.s.d. values of 1.227, 0.338 and 0.470 Å, respectively.

All four inhibitors were cocrystallized with human p38α in the presence of octyl glucoside, and one molecule of the detergent is bound in the lipid-binding pocket in each structure. Significant differences between the four structures are restricted to the ATP-binding pocket, where ligand-induced conformational differences were observed in the hinge region, the Gly-rich loop and the DFG motif.

3.2. Novel X-ray structure of p38α–TAK-715

The structure of p38α–TAK-715 was determined at 1.89 Å resolution (R factor = 17.6%, $R_{\rm free}$ = 23.1%). The binding of TAK-715 to p38α is shown in Fig. 3(*a*). Several interactions are formed to stabilize this complex. The pyridine N atom of the inhibitor makes a hydrogen bond to the main-chain NH of Met109. The amide NH of TAK-715 is hydrogen bonded to the main-chain carbonyl of Met109. The N atom of the thiazole core forms a direct hydrogen bond to the active-site Lys53, which also interacts with Glu71. Lys53 and Asp168 are

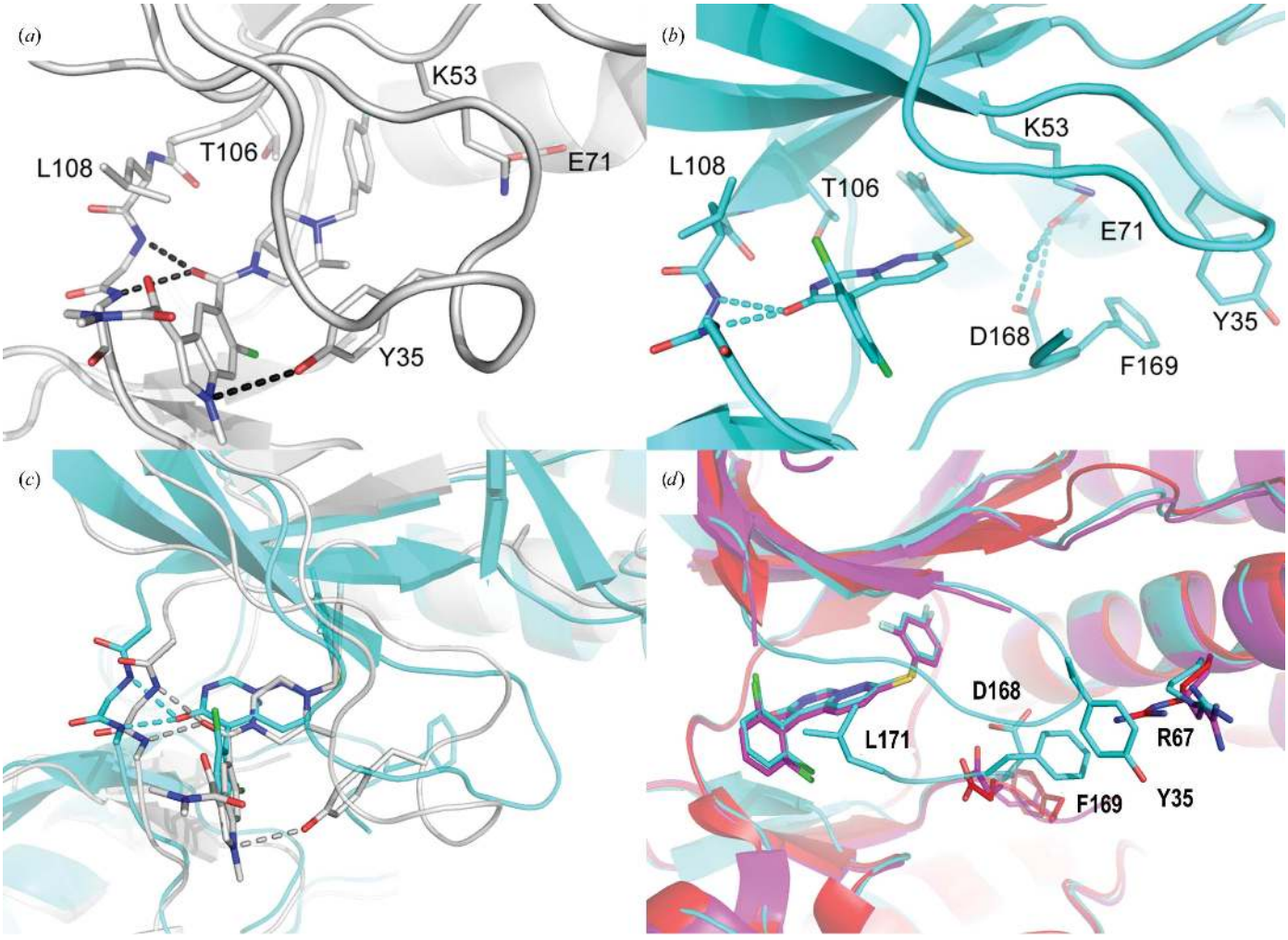

Figure 4
Structures of p38α bound to SCIO-469 and VX-745. Inhibitors and specific amino acids are shown in stick representation and labelled throughout the figure. Hydrogen-bonding interactions are indicated by dotted lines. (*a*) ATP pocket of p38α with bound SCIO-469. (*b*) ATP pocket of p38α with bound VX-745. (*c*) Superposition of structures with SCIO-469 and VX-745. (*d*) Overlay of previously published p38α–VX-745 structures (PDB entry 3fc1, red; PDB entry 3hp5, magenta) and the complex presented here (cyan). Specific residues are labelled to indicate conformational differences (our structure, black; PDB entry 3fc1, magenta)

connected through water-mediated hydrogen bonds. Furthermore, the thiazole core is stacked upon the phenyl side chain of Phe169 and the ethyl group of the thiazole is within van der Waals distance of Tyr35. The 3-methylphenyl moiety binds in the hydrophobic back pocket and the phenyl moiety of the amide is located in the front pocket of p38α, which is planar and hydrophobic in this conformation of the protein. Surprisingly, the DFG group is in a DFG-out conformation even though no detergent molecule is present in the DFG pocket.

3.3. X-ray structure of p38α–SB-203580

The structure of p38α–SB-203580 was determined at 1.7 Å resolution (R factor = 18.3%, $R_{\rm free}$ = 21.6%), the highest resolution published to date. Five structures of p38α bound to this inhibitor are available in the public domain (PDB entries 1a9u, 2ewa, 3gcp, 3obg and 3mpa; Wang *et al.*, 1998; Vogtherr *et al.*, 2006; Simard *et al.*, 2009). Of these, PDB entry 3gcp is the most similar to our structure, with an overall r.m.s.d. between the two structures of 0.261 Å, owing to it being cocrystallized under similar conditions. Nevertheless, and owing to the high resolution, the structure presented here contains more information, including the detailed water-mediated hydrogen-bonding network. The binding of SB-203580 to the active site of p38α is shown in Fig. 3(*b*). In the structure presented here the DFG-motif has a 'DFG-out' conformation facilitating aromatic stacking interactions between the imidazole core of the inhibitor and the phenyl side chain of Phe169 of the DFG sequence. The DFG-out conformation appears to be stabilized by the presence in the DFG pocket of one molecule of the detergent octyl glucoside, which was used as an additive during crystallization. As mentioned previously, the DFG-in conformation observed in PDB entry 1a9u (see comparison in Fig. 3*d*) was obtained *via* a soaking methodology. PDB entry 2ewa is also a soaked complex, but shows a double DFG-in and DFG-out conformation. It appears that soaking prohibits the more stable DFG-out conformation being achieved or stabilized.

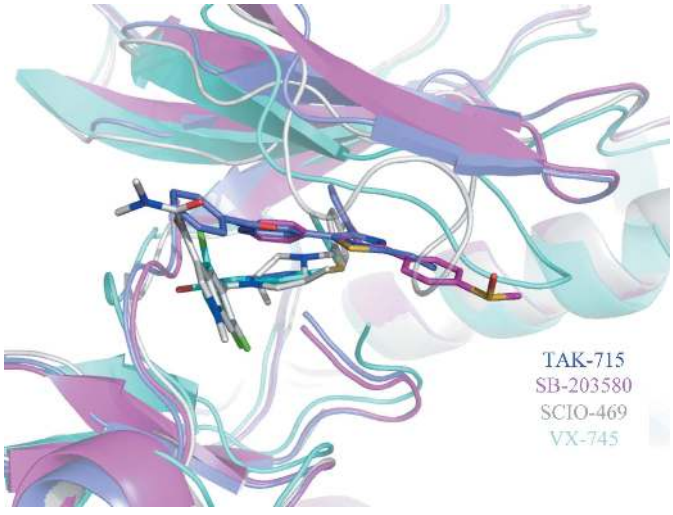

Figure 5
Comparison of the ATP pockets of human p38α bound to SB-203580 (magenta), TAK-715 (blue), SCIO-469 (grey) and VX-745 (cyan).

3.4. X-ray structure of p38α–SCIO-469

The structure of p38α–SCIO-469 was determined at 2.05 Å resolution (R factor = 20.0%, $R_{\rm free}$ = 25.7%) and is similar to the 2.25 Å resolution structure with PDB code 3hub (Simard *et al.*, 2010), with an overall r.m.s.d. between the complexes of 0.303 Å. Two distinguishing features are displayed in this complex, namely the hinge flip and the curling of the Gly-rich loop over the inhibitor.

The central carbonyl O atom of SCIO-469 forms bidentate hydrogen bonds to the main-chain amides of Met109 and Gly110 in the hinge region (Fig. 4*a*). This interaction is facilitated by a peptide flip between these two residues. The dimethylpiperazine does not make any polar interactions with the protein, but makes extensive van der Waals interactions with the side chain of Tyr35; short contacts (2.4 and 2.8 Å) appear to exist between one of the methyl groups of the piperazine and the CB and CG atoms of Tyr35. Density for this methyl is lacking, but neither SCIO-469 nor Tyr35 can be built in alternative conformations. The position of Tyr35 is stabilized by a polar interaction between this residue and the lone pair of the indole N atom of SCIO-469. This conformation of the Gly-rich loop has only previously been observed in a relatively small number of protein kinases, namely Abl (Cowan-Jacob *et al.*, 2007), FGFR1 (Tsai *et al.*, 2008), Met (D'Angelo *et al.*, 2008), EphA3 (PDB entry 3dzq; Structural Genomics Consortium, unpublished work), AurA (PDB entry 3dj5; R. A. Elling, D. Erlanson, W. Yang, B. T. Tangonan, S. K. Hansen & M. J. Romanowski, unpublished work) and p38β (Patel *et al.*, 2009).

3.5. X-ray structure of p38α–VX-745

The structure of p38α–VX-745 (Fig. 4*b*) was determined at 2.4 Å resolution (R factor = 23.06%, $R_{\rm free}$ = 27.07%). This structure is similar to PDB entries 3fc1 (r.m.s.d. of 0.452 Å) and 3hp5 (r.m.s.d. of 0.316 Å) (Pearlman, 2005; Selness *et al.*, 2009) in the way that VX-745 binds to the hinge, back and front pockets (Fig. 4*d*). Even though the resolution is slightly lower than that of 3hp5, some of the features of the protein that were not well defined in the previously published structures are clearly visible in ours, in particular the Gly-rich loop and parts of the activation loop. This might arise from the cocrystallization approach adopted, whereas PDB entry 3hp5 was obtained by soaking experiments. The Gly-rich loop shows an extended conformation, with its edge residue, Tyr35, pointing away from the ATP pocket and occupying the position that Arg67 occupies in PDB entry 3fc1. The conformation of the beginning of the activation loop is markedly different compared with previous structures (in a DFG-in conformation), with the complex presented here showing an uncommon DFG-out conformation. Phe169 is positioned outside the DFG pocket, but points away from the hinge. This conformation is quite rare; it has been observed twice before and only in p38α (Wrobleski *et al.*, 2008). Leu171 points into the

ATP pocket and interacts with the dichlorophenyl group of VX-745 that binds in the front pocket. This means that the ATP pocket is partially closed and that the G-loop and the activation loop are in contact *via* face-to-edge interactions of the side chains of Tyr35 and Phe169.

3.6. Structure comparisons

On the basis of the determination of the four structures presented here, as well as a large number of proprietary p38α–inhibitor structures (data not shown), it has become clear that ligand-induced p38α conformations with a DFG-out state as in Fig. 3 are likely to cocrystallize relatively quickly (1–3 d) and often result in high-resolution structures (1.5–2.5 Å) even using an in-house X-ray radiation source. Conversely, p38α–ligand complexes with a DFG-in conformation often only crystallize after a few weeks and diffract relatively weakly, *i.e.* to about 2.5–3.0 Å. Consistent with these observations, the structures presented here show that the DFG-out conformations (Fig. 3) have a relatively compact structure with a 'low' Gly-rich loop and aromatic stacking interactions between inhibitor, Tyr35 and Phe169, whereas the DFG-in conformations contain a 'high' Gly-rich loop that exhibits far fewer interactions with the relevant inhibitors (Fig. 4). As cocrystallization was conducted under identical conditions, these and other structural differences between the four protein–ligand structures can be attributed to ligand induction, enabling a thorough comparison of the structural details and coupling to kinase selectivity profiles.

Comparison of the four ATP regions shows that the protein conformations cluster into two groups: one group comprises TAK-715 and SB-203580, while the other contains SCIO-469 and VX-745 (Fig. 5). SB-203580 and TAK-715 bind relatively 'high' in the ATP pocket, occupying the hydrophobic back pocket, the adenine region and the front pocket of p38α as well as extending to most of the length of the Gly-rich loop, compared with the other two compounds, which mostly bind in the back, adenine and front pockets. Consequently, the Gly-rich loop in the former two structures is pushed upward in an open conformation, whereas this loop adopts a 'closed' conformation upon binding SCIO-469 and VX-745. The only interaction conserved in all four structures is that between a substituted phenyl in each compound and the hydrophobic back pocket of p38α.

The binding modes of SB-203580 and TAK-715 to p38α are shown in Fig. 3(*d*). Both molecules bind to similar areas of the ATP pocket such as the adenine, sugar and back-pocket regions and both compounds induce DFG-out and Tyr35-in conformations, resulting in a relatively flat ATP pocket. The only significant difference is the fact that TAK-715 reaches further into the front pocket through its benzamide group, whereas SB-203580 does not.

The compounds in the other cluster, SCIO-469 and VX-745, bind similarly and induce similar protein conformations (Fig. 4*c*). Both compounds interact with the hinge, front and back pockets but do not contact the sugar- and phosphate-binding regions. A peptide flip is induced in the hinge, which results in the presentation of two hydrogen-bond donors in the ATP pocket, a clear difference from the acceptor–donor–acceptor pattern normally present in the ATP pocket of protein kinases. It has been noted previously that the peptide flip is energetically accessible by the presence of a glycine residue (Gly110) at the appropriate position in the hinge (Xing *et al.*, 2009), that this residue is specific to the α-, β- and γ-isoforms of p38 and that this feature could be exploited in future p38-inhibitor design (Fitzgerald *et al.*, 2003). Analysis of the PDB shows that this peptide flip has been observed previously in p38α (Xing *et al.*, 2009) and in the protein kinases haspin (Eswaran *et al.*, 2009) and ERK2 (Kinoshita *et al.*, 2006). Haspin is indeed one of 42 kinases that exhibit a glycine residue at the relevant position (Manning *et al.*, 2002). In ERK2, the peptide flip of Glu109 in the position equivalent to Gly110 is tolerated because two disadvantageous factors in the binding of the compound are settled by this motion (Kinoshita *et al.*, 2006). The recently reported p38 inhibitor PH-797804 induces a peptide flip similar to that observed in the VX-745 and SCIO-469 complexes (Xing *et al.*, 2009).

The most significant differences between the two structures are the conformations of the Gly-rich loop and the DFG segment. The Gly-rich loop is completely curled up in the SCIO-469 structure but adopts a strand–turn–strand structure upon binding VX-745. The DFG motif is in an unusual DFG-out conformation in the p38α–VX-745 complex, with the Phe169 side chain pointing towards the αC helix.

3.7. Structure–selectivity relationships

The four inhibitors discussed in this paper induce different protein conformations and make contacts with different residues. In addition, the inhibitors exhibit different kinase selectivity profiles.

SB-203580 shows limited selectivity, as determined by profiling 38 protein kinase inhibitors in an assay panel comprising 317 human protein kinases (Karaman *et al.*, 2008). SB-203580 was found to inhibit kinase activity with values below 1 μM in 18 assays and below 10 μM in 43 assays. The targets inhibited were distributed across all subfamilies in the kinome. This relative lack of selectivity may be explained using the X-ray structure described here. The compound is bound mostly in regions that are conserved in protein kinases for the binding of ATP. The only group that extends into regions unrelated to function and thus divergent in kinase structures is the fluorophenyl group, which binds into the back pocket *via* the gatekeeper residues Thr106 and Lys53. This will generate selectivity against kinases that contain large gatekeeper residues. In the kinome, the majority of enzymes (72%) have medium large to large gatekeepers. These kinases (with, for example, Phe, Trp or Tyr gatekeepers) are indeed unable to bind SB-203580 with high affinity. Of the 19 kinases strongly inhibited by SB-203580, 12 contain a small Thr and seven a medium-sized (but flexible) Met gatekeeper, both of which allow access to the back pocket. Another interaction between p38 and SB-203580 is the aromatic stacking interaction between the phenyl group of the inhibitor and Tyr35,

which points into the ATP pocket. Some 84% of the kinome contains a Tyr (21%) or Phe (63%) that would facilitate a similar interaction. Clearly, the interaction with Tyr35 does not contribute greatly to kinase selectivity.

Based on the structure comparison between SB-203580 and TAK-715, TAK-715 may be expected to be more selective than SB-203580 as it extends further into the front pocket (Fig. 3*c*). TAK-715 has been reported to be selective over several other kinases, including isoforms p38γ and p38δ (Miwatashi *et al.*, 2005). However, more recent analysis of the selectivity of TAK-715 over a wider range of human protein kinases showed this compound to be relatively nonselective.

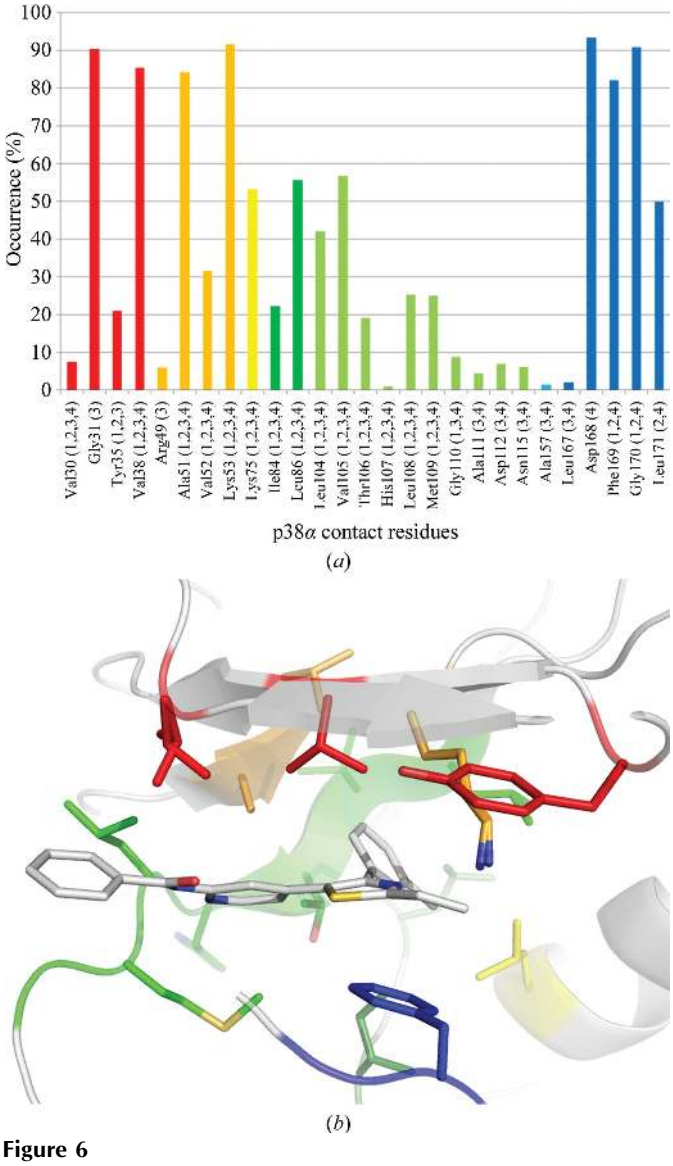

Figure 6
(*a*) Occurrence of p38α contact residues in the presented structures, *i.e.* residues that are within 4 Å distance of any of the four ligands in these p38α cocrystal structures. The occurrence (in %) of each contact residue in the human protein kinase multiple sequence alignment is given. Contacts with (1) TAK-715, (2) SB-203580, (3) SCIO-469 and (4) VX-745 are indicated for each residue. (*b*) Mapping of contact residues of TAK-715 onto the complex structure. Different colours represent different subdomains from the Hunter classification (Hanks & Hunter, 1995; not shown).

TAK-715 was reported to inhibit 22 kinases by more than 80% when screened at 10 μM (Verkaar *et al.*, 2011). The five specified kinases all contained Thr or Met gatekeepers and thus a similar pattern to that observed for SB-203580 appears to exist for selectivity and gatekeeper identity. Analysis of X-ray structures and contact residues (see below) shows that there is little structural difference between TAK-715 and SB-203580. For TAK-715, the contact-residue analysis (cutoff at 4 Å) indicates one extra interaction with Gly110 at the end of the hinge, while the X-ray structure indicates some longer range hydrophobic interactions with the front benzamide of the inhibitor. Overall, the type and numbers of protein–ligand interactions are similar for both the SB-203580 and TAK-715 complexes and this is reflected in similar kinase-selectivity profiles.

Both SCIO-469 and VX-745 are highly selective p38α inhibitors (Karaman *et al.*, 2008; Verkaar *et al.*, 2011). The compounds do not use all of the subpockets of the ATP-binding region, but their interactions are optimized. In fact, for SCIO-469 the only polar interactions observed are those (i) between the carbonyl and the hinge and (ii) between the substituted piperazine and the adenine region. Instead, substantial hydrophobic interactions are observed in the front and back pocket regions, two regions that are diverse in protein kinases as they are not required for function/catalysis. SCIO-469 has the extra amide group bound to the front pocket, which could also interact with Arg49 of subdomain II. This residue was identified as one of the contact residues differing from those of VX-745 in our analysis.

The shape and properties of the front pocket in this protein conformation are also a consequence of the main-chain peptide flip that is observed in the hinge region between Met109 and Gly110 for both SCIO-469 and VX-745. This peptide flip is accessible because of the presence of Gly110, which increases the conformational space around this residue. Induction of the peptide flip is a feature shared by SCIO-469, VX-745 and PH-797804. As all of these compounds have been reported to be highly selective for p38, it is highly likely that inhibitor-driven induction of the hinge flip is a major contributor to selectivity. The curled conformation of the Gly-rich loop should also add to the selectivity of SCIO-469, as this conformation is stabilized by interaction with the ligand.

Previously, it has been claimed that adoption of the inactive DFG-out conformation would correlate with improved selectivity (Liu & Gray, 2006; Mol *et al.*, 2004; Simard *et al.*, 2009). This cannot be confirmed from this study, as the least selective compounds both show this fold whilst SCIO-469 does not and VX-745 has either an 'in' conformation or an unusual 'out' position.

Analysis of the contact residues that are within a distance of 4 Å of these four ligands (Fig. 6*a*) shows that both TAK-715 (Fig. 6*b*) and SB-203580 make a total of 18 contacts with the protein, whilst SCIO-469 and VX-745 make 23 and 24 interactions, respectively. For these inhibitors, the relatively large number of contact residues results in improved selectivity, as the combination of interactions becomes more kinase-specific with a larger numbers of contacts. For a more specific deter-

mination of the contribution of each of these residues, they were implemented in the human eukaryotic protein kinase (ePK) multiple sequence alignment (http://kinase.com/human/kinome/groups/ePK.aln; Manning *et al.*, 2002). This enables calculation of how often each of these residues occurs in the human kinome (Fig. 6*a*). The major differences between VX-745/SCIO-469 and SB-203580/TAK-715 are the interactions at the end of the hinge and in the front pocket. In addition to inducing the hinge flip, the more selective compounds occupy a larger volume in the front pocket, making contacts with Ala111, Asp112 and Asn115. Each of these three residues has an occurrence of less than 10% at these positions in the kinome, making them hotspots for improving kinase selectivity towards p38α. To relate the measured kinase selectivity to the underlying protein–ligand interactions, the average occurrence of contact residues in the kinome was calculated for each of the four inhibitors described in this paper. The average occurrences for SB-203580, TAK-715, VX-745 and SCIO-469 were 47, 45, 39 and 32%, respectively. Once again, this correlates well with their selectivity profiles, as VX-745 and SCIO-469 have more interactions with amino acids that occur less often in the kinome. These calculations were also performed for the MAPK subset of the human kinome. As expected, the occurrences of the contact residues are higher in the MAPK subset (70, 66, 64 and 58%, respectively) but the overall trend is the same.

In conclusion, we present the X-ray structures of four p38α–inhibitor complexes, one of which is presented for the first time, and relate the protein conformation to observed kinase selectivity profiles. We show that the choice of experimental conditions, in particular the use of cocrystallization rather than soaking, has a significant impact on the conformation of p38α–inhibitor complexes. For this reason, we advise that not only the structures of inhibitors in complex with the protein kinase of interest should be determined, but that the crystallization of public domain complexes under the same conditions should also be attempted whenever possible in order to be able to extract meaningful comparisons between structures. The highly selective p38α inhibitors SCIO-469 and VX-745 induce an unusual peptide flip. SCIO-469 also induces a collapsed Gly-rich loop, whilst the DFG sequence in VX-745 adopts the rare DFG-out conformation. Contact-residue analysis shows that the latter two inhibitors make more interactions with the protein than the less selective inhibitors SB-203580 and TAK-715 and make more interactions with residues that are less conserved within the human kinome.

We thank Joost Uitdehaag for generation of the expression construct for p38α and Wim Koot for performing large-scale fermentor expression cultures.

References

Akella, R., Min, X., Wu, Q., Gardner, K. H. & Goldsmith, E. J. (2010). *Structure*, **18**, 1571–1578.

Brünger, A. T. (1992). *Nature (London)*, **355**, 472–475.

Bukhtiyarova, M., Northrop, K., Chai, X., Casper, D., Karpusas, M. & Springman, E. (2004). *Protein Expr. Purif.* **37**, 154–161.

Chang, C.-I., Xu, B., Akella, R., Cobb, M. H. & Goldsmith, E. J. (2002). *Mol. Cell*, **9**, 1241–1249.

Cowan-Jacob, S. W., Fendrich, G., Floersheimer, A., Furet, P., Liebetanz, J., Rummel, G., Rheinberger, P., Centeleghe, M., Fabbro, D. & Manley, P. W. (2007). *Acta Cryst.* D**63**, 80–93.

D'Angelo, N. D. *et al.* (2008). *J. Med. Chem.* **51**, 5766–5779.

Emsley, P. & Cowtan, K. (2004). *Acta Cryst.* D**60**, 2126–2132.

Eswaran, J., Patnaik, D., Filippakopoulos, P., Wang, F., Stein, R. L., Murray, J. W., Higgins, J. M. & Knapp, S. (2009). *Proc. Natl Acad. Sci. USA*, **106**, 20198–20203.

Evans, P. (2006). *Acta Cryst.* D**62**, 72–82.

Fitzgerald, C. E., Patel, S. B., Becker, J. W., Cameron, P. M., Zaller, D., Pikounis, V. B., O'Keefe, S. J. & Scapin, G. (2003). *Nature Struct. Biol.* **10**, 764–769.

Freshney, N. W., Rawlinson, L., Guesdon, F., Jones, E., Cowley, S., Hsuan, J. & Saklatvala, J. (1994). *Cell*, **78**, 1039–1049.

Genovese, M. C. (2009). *Arthritis Rheum.* **60**, 317–320.

Hammaker, D. & Firestein, G. S. (2010). *Ann. Rheum. Dis.* **69**, i77–i82.

Han, J., Jiang, Y., Li, Z., Kravchenko, V. V. & Ulevitch, R. J. (1997). *Nature (London)*, **386**, 296–299.

Han, J., Lee, J. D., Bibbs, L. & Ulevitch, R. J. (1994). *Science*, **265**, 808–811.

Hanks, S. K. & Hunter, T. (1995). *FASEB J.* **9**, 576–596.

Karaman, M. W. *et al.* (2008). *Nature Biotechnol.* **26**, 127–132.

Kinoshita, T., Warizaya, M., Ohori, M., Sato, K., Neya, M. & Fujii, T. (2006). *Bioorg. Med. Chem. Lett.* **16**, 55–58.

Krieger, E., Koraimann, G. & Vriend, G. (2002). *Proteins*, **47**, 393–402.

Lee, J. C. *et al.* (1994). *Nature (London)*, **372**, 739–746.

Liu, Y. & Gray, N. S. (2006). *Nature Chem. Biol.* **2**, 358–364.

MacNee, W., Allan, R., Jones, I., De Salvo, M. C. & Tan, L. (2010). *Eur. Respir. J.* **36**, Suppl. 54, 718s.

Maini, R., St Clair, E. W., Breedveld, F., Furst, D., Kalden, J., Weisman, M., Smolen, J., Emery, P., Harriman, G., Feldmann, M. & Lipsky, P. (1999). *Lancet*, **354**, 1932–1939.

Manning, G., Whyte, D. B., Martinez, R., Hunter, T. & Sudarsanam, S. (2002). *Science*, **298**, 1912–1934.

Miwatashi, S., Arikawa, Y., Kotani, E., Miyamoto, M., Naruo, K., Kimura, H., Tanaka, T., Asahi, S. & Ohkawa, S. (2005). *J. Med. Chem.* **48**, 5966–5979.

Mol, C. D., Fabbro, D. & Hosfield, D. J. (2004). *Curr. Opin. Drug Discov. Devel.* **7**, 639–648.

Murshudov, G. N., Skubák, P., Lebedev, A. A., Pannu, N. S., Steiner, R. A., Nicholls, R. A., Winn, M. D., Long, F. & Vagin, A. A. (2011). *Acta Cryst.* D**67**, 355–367.

Nishimoto, N., Miyasaka, N., Yamamoto, K., Kawai, S., Takeuchi, T., Azuma, J. & Kishimoto, T. (2009). *Mod. Rheumatol.* **19**, 12–19.

Patel, S. B., Cameron, P. M., O'Keefe, S. J., Frantz-Wattley, B., Thompson, J., O'Neill, E. A., Tennis, T., Liu, L., Becker, J. W. & Scapin, G. (2009). *Acta Cryst.* D**65**, 777–785.

Pearlman, D. A. (2005). *J. Med. Chem.* **48**, 7796–7807.

Rouse, J., Cohen, P., Trigon, S., Morange, M., Alonso-Llamazares, A., Zamanillo, D., Hunt, T. & Nebreda, A. R. (1994). *Cell*, **78**, 1027–1037.

Selness, S. R. *et al.* (2009). *Bioorg. Med. Chem. Lett.* **19**, 5851–5856.

Simard, J. R., Getlik, M., Grütter, C., Pawar, V., Wulfert, S., Rabiller, M. & Rauh, D. (2009). *J. Am. Chem. Soc.* **131**, 13286–13296.

Simard, J. R., Getlik, M., Grütter, C., Schneider, R., Wulfert, S. & Rauh, D. (2010). *J. Am. Chem. Soc.* **132**, 4152–4160.

Tong, L., Pav, S., White, D. M., Rogers, S., Crane, K. M., Cywin, C. L., Brown, M. L. & Pargellis, C. A. (1997). *Nature Struct. Biol.* **4**, 311–316.

Tsai, J. *et al.* (2008). *Proc. Natl Acad. Sci. USA*, **105**, 3041–3046.

Verkaar, F., van der Doelen, A. A., Smits, J. F., Blankesteijn, W. M. & Zaman, G. J. (2011). *Chem. Biol.* **18**, 485–494.

Vogtherr, M., Saxena, K., Grimme, S., Betz, M., Schieborr, U., Pescatore, B., Langer, T. & Schwalbe, H. (2005). *J. Biomol. NMR*, **32**, 175.

Vogtherr, M., Saxena, K., Hoelder, S., Grimme, S., Betz, M., Schieborr, U., Pescatore, B., Robin, M., Delarbre, L., Langer, T., Wendt, K. U. & Schwalbe, H. (2006). *Angew. Chem. Int. Ed. Engl.* **45**, 993–997.
Wang, Z., Canagarajah, B. J., Boehm, J. C., Kassisà, S., Cobb, M. H., Young, P. R., Abdel-Meguid, S., Adams, J. L. & Goldsmith, E. J. (1998). *Structure*, **6**, 1117–1128.
Wang, Z., Harkins, P. C., Ulevitch, R. J., Han, J., Cobb, M. H. & Goldsmith, E. J. (1997). *Proc. Natl Acad. Sci. USA*, **94**, 2327–2332.
Wilson, K. P., Fitzgibbon, M. J., Caron, P. R., Griffith, J. P., Chen, W., McCaffrey, P. G., Chambers, S. P. & Su, M. S.-S. (1996). *J. Biol. Chem.* **271**, 27696–27700.
Winn, M. D. *et al.* (2011). *Acta Cryst.* D**67**, 235–242.
Wrobleski, S. T. *et al.* (2008). *Bioorg. Med. Chem. Lett.* **18**, 2739–2744.
Xing, L. *et al.* (2009). *Biochemistry*, **48**, 6402–6411.